The water-soluble Re_6-clusters with aromatic phosphine ligands – from synthesis to potential biomedical applications

Anton A. Ivanov,[a,b] Dmitry I. Konovalov,[a,c] Tatiana N. Pozmogova,[b,c,d] Anastasiya O. Solovieva,[b,d] Anatoly R. Melnikov,[c,e] Konstantin A. Brylev,[a,c] Natalia V. Kuratieva,[a,c] Vadim V. Yanshole,[c,f] Kaplan Kirakci,[g] Kamil Lang,[g] Svetlana N. Cheltygmasheva,[b] Noboru Kitamura,[h] Lidiya V. Shestopalova,[c] Yuri V. Mironov[a,c] and Michael A. Shestopalov[a,b,c,d]*

[a.] *Nikolaev Institute of Inorganic Chemistry SB RAS, 3 Acad. Lavrentiev Ave., 630090 Novosibirsk, Russia.*
[b.] *Federal Research Center of Fundamental and Translational Medicine, 2 Timakova str., 630117 Novosibirsk, Russia.*
[c.] *Novosibirsk State University, 2 Pirogova str., 630090 Novosibirsk, Russia.*
[d.] *Scientific Institute of Clinical and Experimental Lymphology – branch of ICG SB RAS, 2 Timakova str., 630060 Novosibirsk, Russia.*
[e.] *Voevodsky Institute of Chemical Kinetics and Combustion SB RAS, 3 Institutskaya st., Novosibirsk, 630090, Russia.*
[f.] *International Tomography Center SB RAS, 3a Institutskaya St., 630090 Novosibirsk, Russia.*
[g.] *Institute of Inorganic Chemistry of the Czech Academy of Sciences, v.v.i., Husinec-Řež 1001, 250 68 Řež, Czech Republic.*
[h.] *Department of Chemistry, Faculty of Science, Hokkaido University, 060-0810 Sapporo, Japan.*

Table of content:

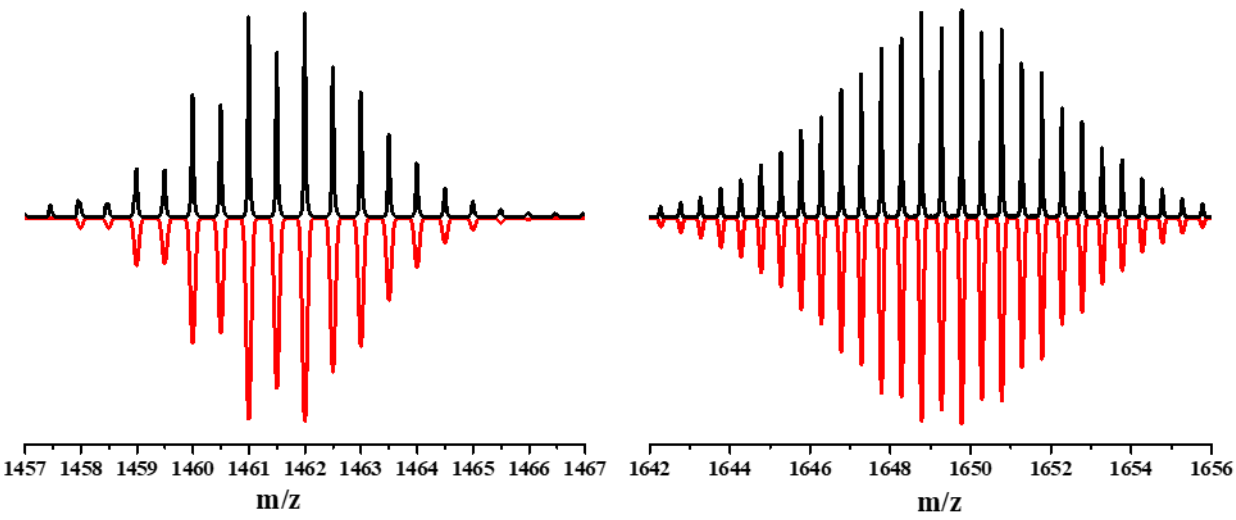

Figure 1S. HR-ESI-MS of H_4-**1**·2HBr (left, m/z = 1461.9931) and H_4-**2**·2HBr (right, m/z = 1649.7751) in acetone (black) and the simulation of $[\{Re_6Q_8\}(PPh_2CH_2CH_2COOH)_6]^{2+}$ clusters (Q = S (m/z = 1461.9959) and Se (m/z = 1649.7768)) (red).

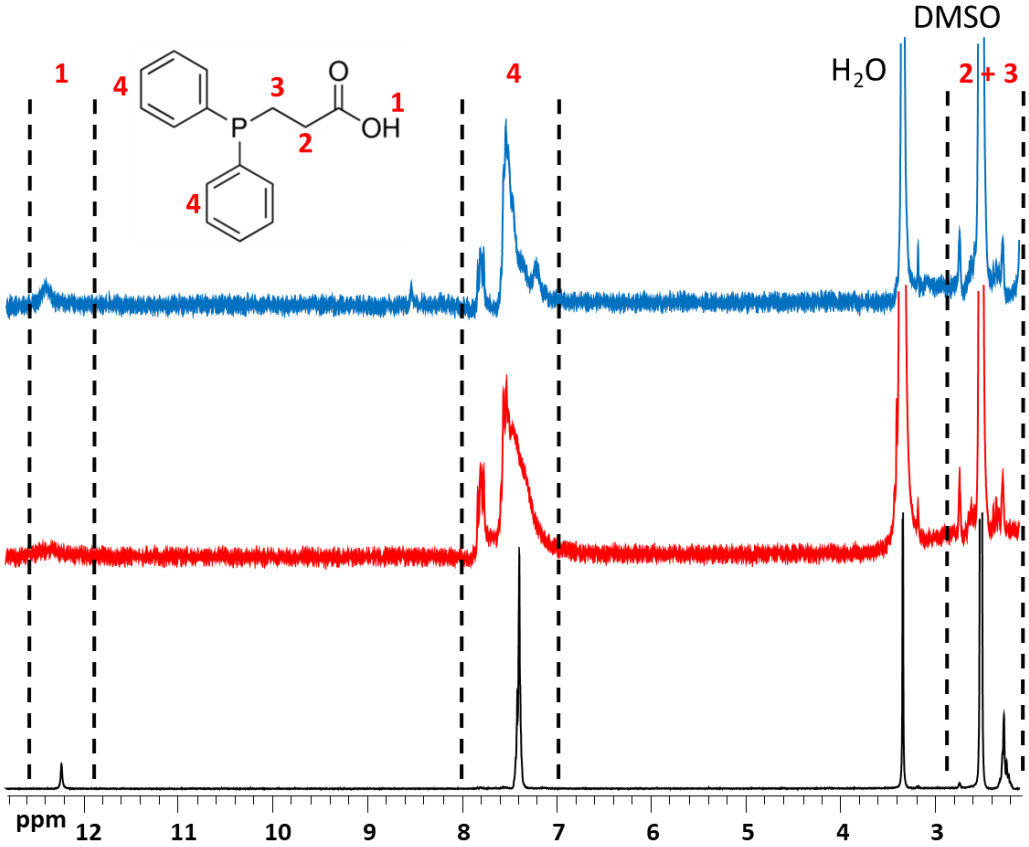

Figure 2S. ^{1}H NMR spectra of (2-carboxyethyl)diphenylphosphine (black), **1**·2HBr·H_2O (red) and H_4-**2**·2HBr·H_2O (blue) in DMSO-d_6.

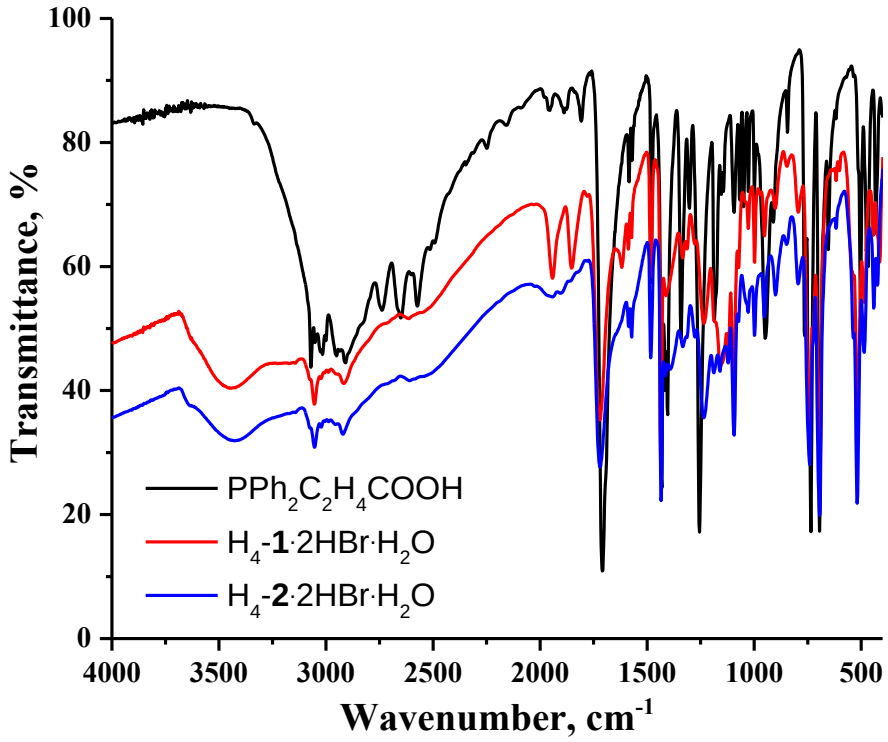

Figure 3S. FTIR spectra of H_4-**1**·2HBr·H_2O and H_4-**2**·2HBr·H_2O compared with that of the ligands, i.e., (2-carboxyethyl)diphenylphosphine.

Table 1S. Crystal data and experimental details for $[\{Re_6Se_8\}(PPh_2CH_2CH_2COOH)_6]Br_2\cdot 6H_2O\cdot Et_2O$ (H_4-**2**$\cdot$2HBr$\cdot$6$H_2O\cdot Et_2O$), $Na_4[\{Re_6S_8\}(PPh_2CH_2CH_2COO)_6]$ (Na_4-**1**$\cdot$4H_2O), and $Na_4[\{Re_6Se_8\}(PPh_2CH_2CH_2COO)_6]$ (Na_4-**2**$\cdot$4H_2O).

Parameter	H_4-**2**$\cdot$2HBr$\cdot$6$H_2O\cdot Et_2O$	Na_4-**1**$\cdot$4H_2O	Na_4-**2**$\cdot$4H_2O
Empirical formula	$C_{94}H_{112}Br_2O_{19}P_6Re_6Se_8$	$C_{90}H_{92}Na_4O_{16}P_6Re_6S_8$	$C_{90}H_{92}Na_4O_{16}P_6Re_6Se_8$
Formula weight	3640.35	3081.09	3456.29
Crystal system	Hexagonal	Triclinic	Triclinic
Space group	$R\bar{3}c$	$P\bar{1}$	$P\bar{1}$
Z	6	1	1
T (K)	150(2)	150(2)	150(2)
a (Å)	17.6727(5)	13.9958(3)	14.1316(15)
b (Å)	17.6727(5)	14.5841(3)	14.6796(15)
c (Å)	75.9637 (19)	14.8362(4)	14.8908(15)
V (Å)	20546.7(13)	2374.12(10)	2374.12(10)
α (º)	90	61.351(1)	60.961(3)
β (º)	90	78.554(1)	78.277(3)
γ (º)	120	63.323(1)	63.097(3)
D_{calc} (g cm^{-3})	1.765	2.155	2.384
μ (mm^{-1})	8.110	7.977	10.715
Crystal size (mm)	0.395 × 0.195 × 0.185	0.20 × 0.12 × 0.10	0.20 × 0.20 × 0.16
ϑ scan range (º)	1.709 to 26.372	2.283 to 26.371	1.564 to 28.426
Indices ranges	$-22 \le h \le 22$ $-21 \le k \le 22$ $-94 \le l \le 93$	$-17 \le h \le 17$ $-18 \le k \le 17$ $-18 \le l \le 18$	$-18 \le h \le 18$ $-19 \le k \le 19$ $-19 \le l \le 18$
Reflections collected	52436	20301	21291
Independent reflections	4675	9667	11836
Observed reflections [I > 2σ(I)]	4134	8955	10372
Parameters	236	603	601
R_{int}	0.0256	0.0304	0.0181
Goodness-of-fit (GOF) on F^2	1.116	1.028	1.055
R_1^a/wR_2^b [I > 2σ(I)]	0.0355/0.0979	0.0192/0.0464	0.0205/0.0467
R_1^a/wR_2^b (all data)	0.0433/0.1034	0.0215/0.0472	0.0261/0.0486
$\Delta\rho_{max}/\Delta\rho_{min}$ (e·Å^{-3})	1.986/–1.316	1.274/–1.004	1.631/–1.037

Table 2S. Selected interatomic distances (Å) for $[\{Re_6Se_8\}(PPh_2CH_2CH_2COOH)_6]Br_2\cdot 6H_2O\cdot Et_2O$ (H_4-**2**$\cdot$2HBr$\cdot 6H_2O\cdot Et_2O$), $Na_4[\{Re_6S_8\}(PPh_2CH_2CH_2COO)_6]\cdot 4H_2O$ (Na_4-**1**$\cdot 4H_2O$), and $Na_4[\{Re_6Se_8\}(PPh_2CH_2CH_2COO)_6]\cdot 4H_2O$ (Na_4-**2**$\cdot 4H_2O$).

Compound	Re–Re (Å)	Re–Q (Å)	Re–P (Å)
H_4-**2**$\cdot$2HBr$\cdot 6H_2O\cdot Et_2O$	2.6389(4)–2.6455(4)	2.5060(7)–2.5244(6)	2.4807(15)
Na_4-**1**$\cdot 4H_2O$	2.60495(16)–2.61506(15)	2.3864(7)–2.4129(7)	2.4842(8)–2.4913(7)
Na_4-**2**$\cdot 4H_2O$	2.6363(3)–2.6515(3)	2.4994(4)–2.5269(4)	2.4849(8)–2.4909(8)

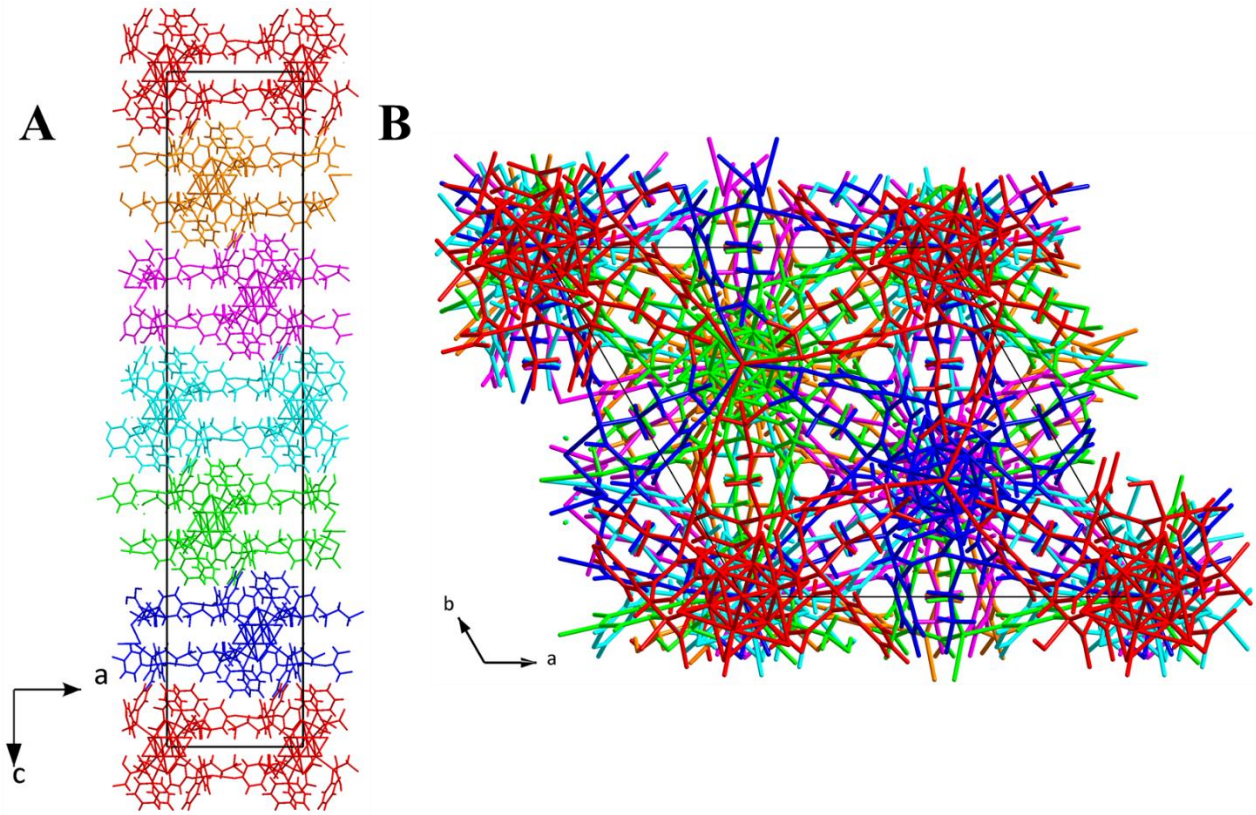

Figure 4S. Layers parallel to the *ab* plane observed in the H_4-**2**$\cdot$2HBr$\cdot 6H_2O\cdot Et_2O$ structure.

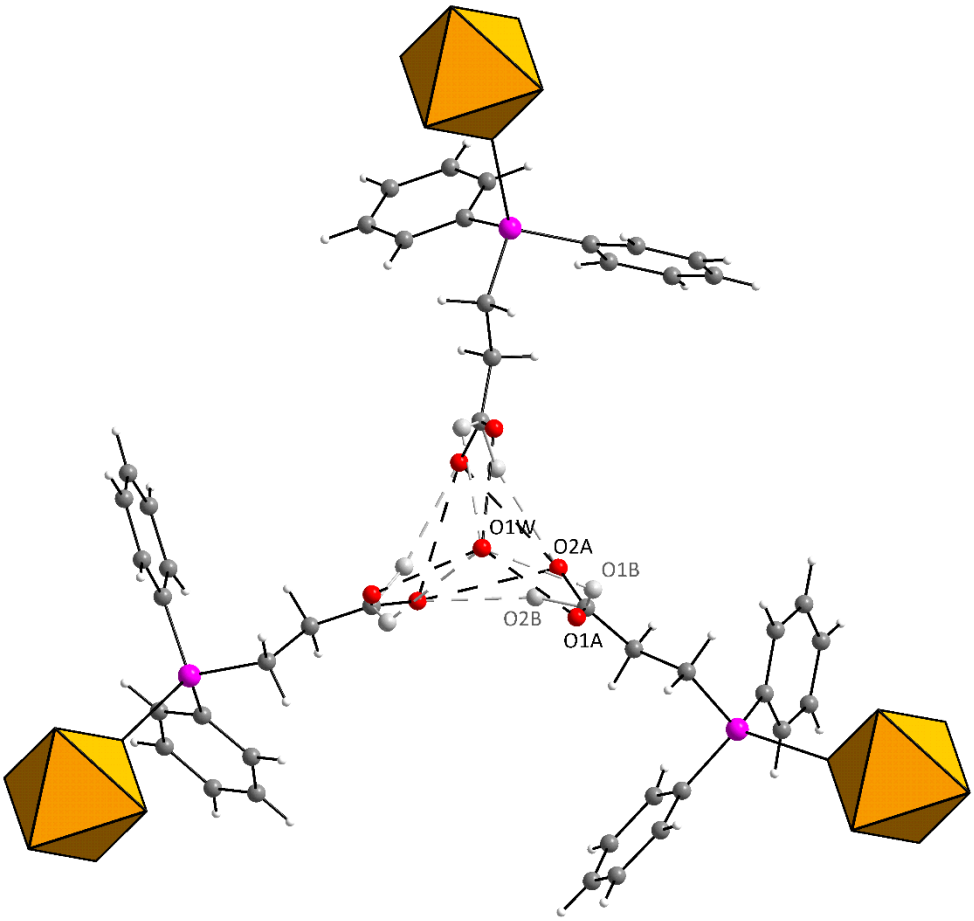

Figure 5S. Hydrogen bonds observed in the H_4-**2**·2HBr·6H_2O·Et_2O structure.

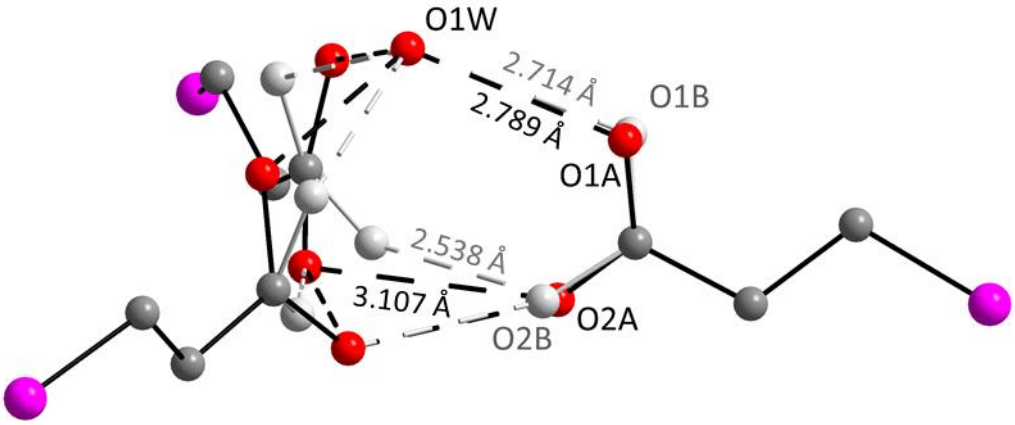

Figure 6S. Hydrogen bonds observed in the H_4-**2**·2HBr·6H_2O·Et_2O structure.

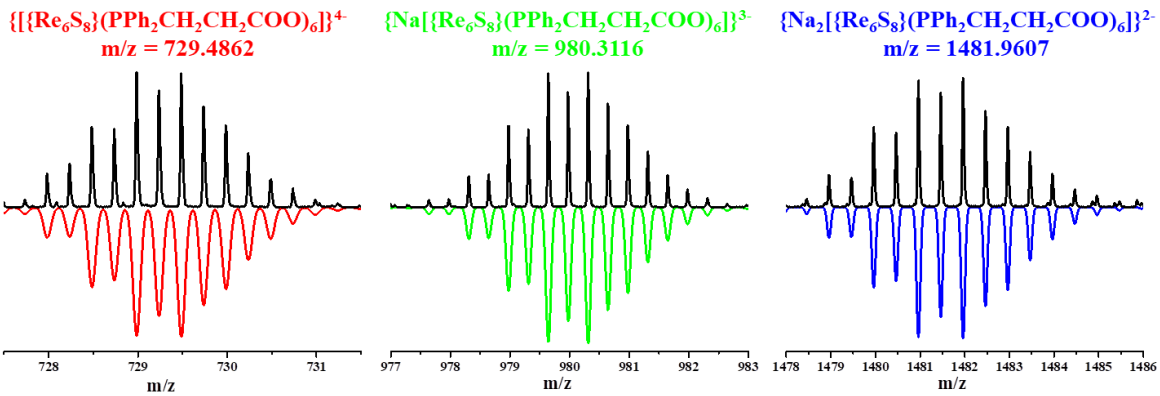

Figure 7S. HR-ESI-MS of Na_4-**1**·$18H_2O$ in water (black) and corresponding simulations of $\{Na_x[\{Re_6S_8\}(PPh_2CH_2CH_2COO)_6]\}^{4-x}$ (x = 0, m/z = 729.4872; x = 1, m/z = 980.3126; x = 2, m/z = 1481.9633) (coloured).

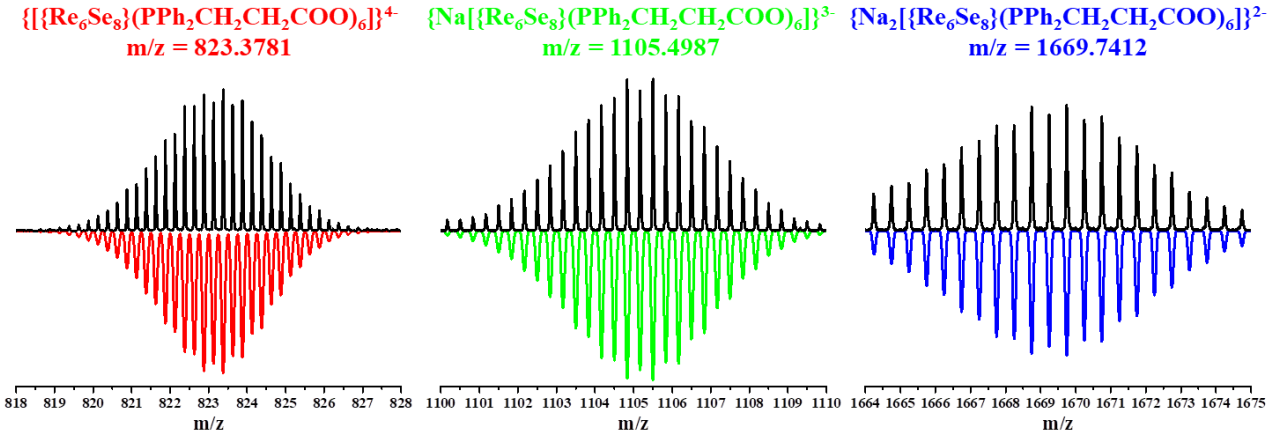

Figure 8S. HR-ESI-MS of Na_4-**2**·$16H_2O$ in water (black) and a simulation of cluster forms $Na_x[\{Re_6Se_8\}(PPh_2CH_2CH_2COO)_6]^{4-x}$ (x = 0 (m/z = 823.3777), 1 (m/z = 1105.4996)) and 2 (m/z = 1669.7442) (coloured).

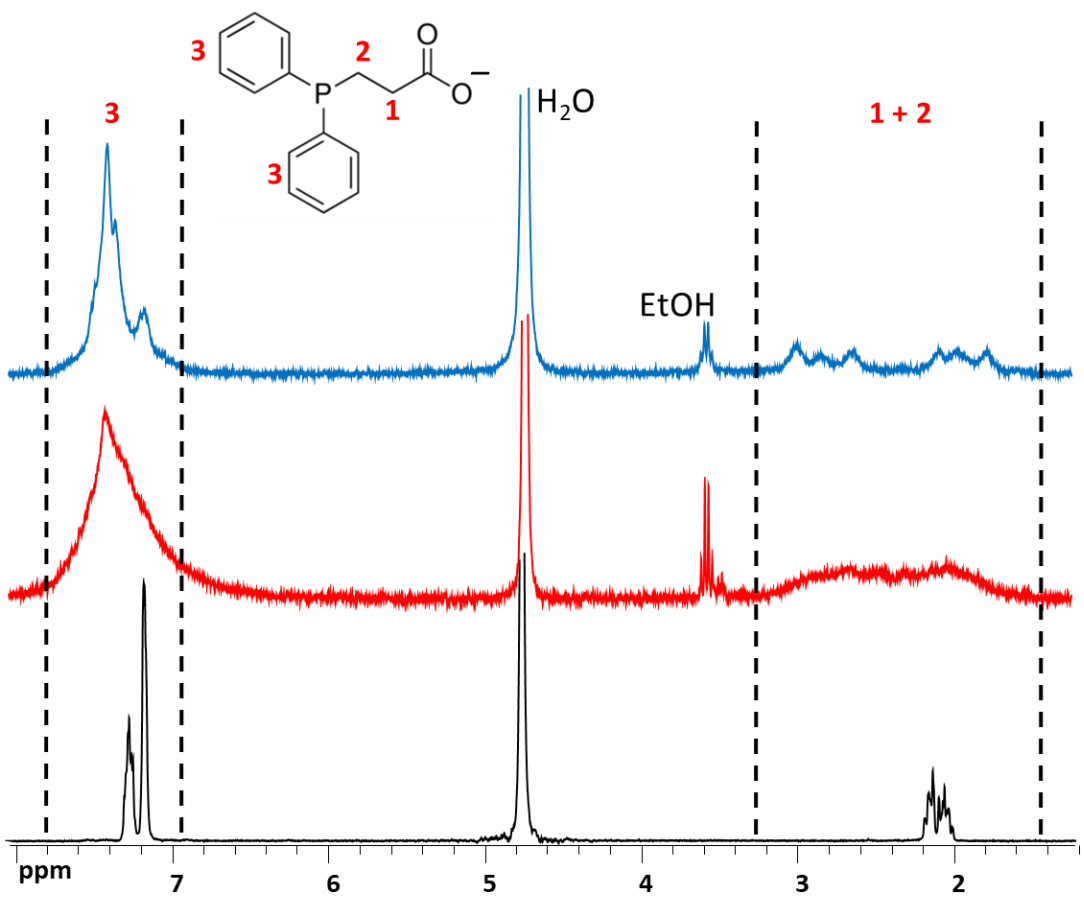

Figure 9S. ^{1}H NMR spectra of (2-carboxyethyl)diphenylphosphine sodium salt (black), Na_4-**1**·$18H_2O$ (red) and Na_4-**2**·$16H_2O$ (blue) in D_2O.

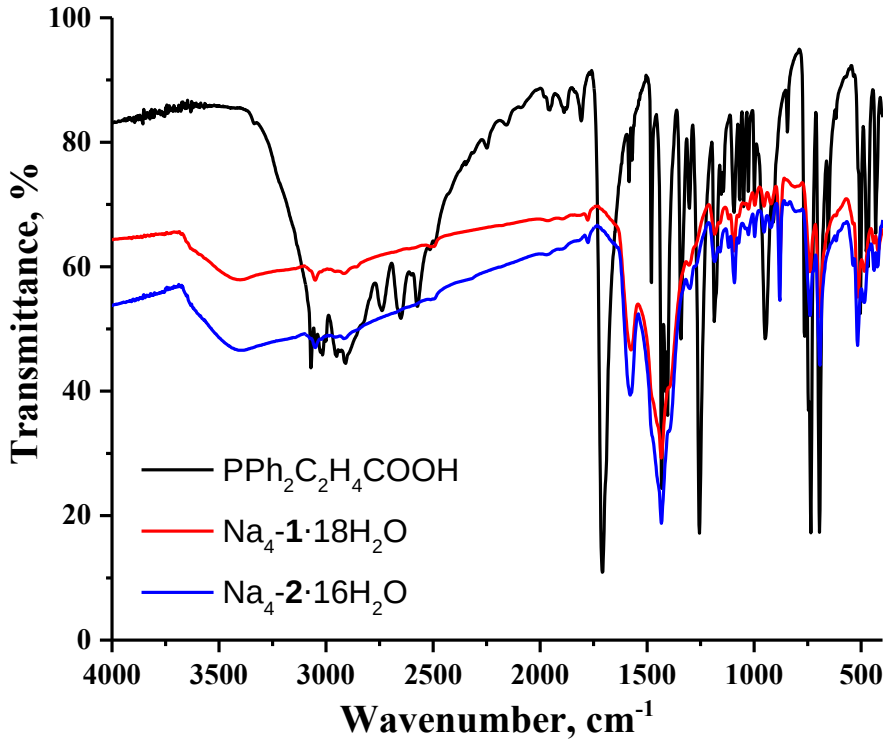

Figure 10S. FTIR spectra of Na_4-**1**·$18H_2O$ and Na_4-**2**·$16H_2O$ compared with that of the ligands, i.e., (2-carboxyethyl)diphenylphosphine.

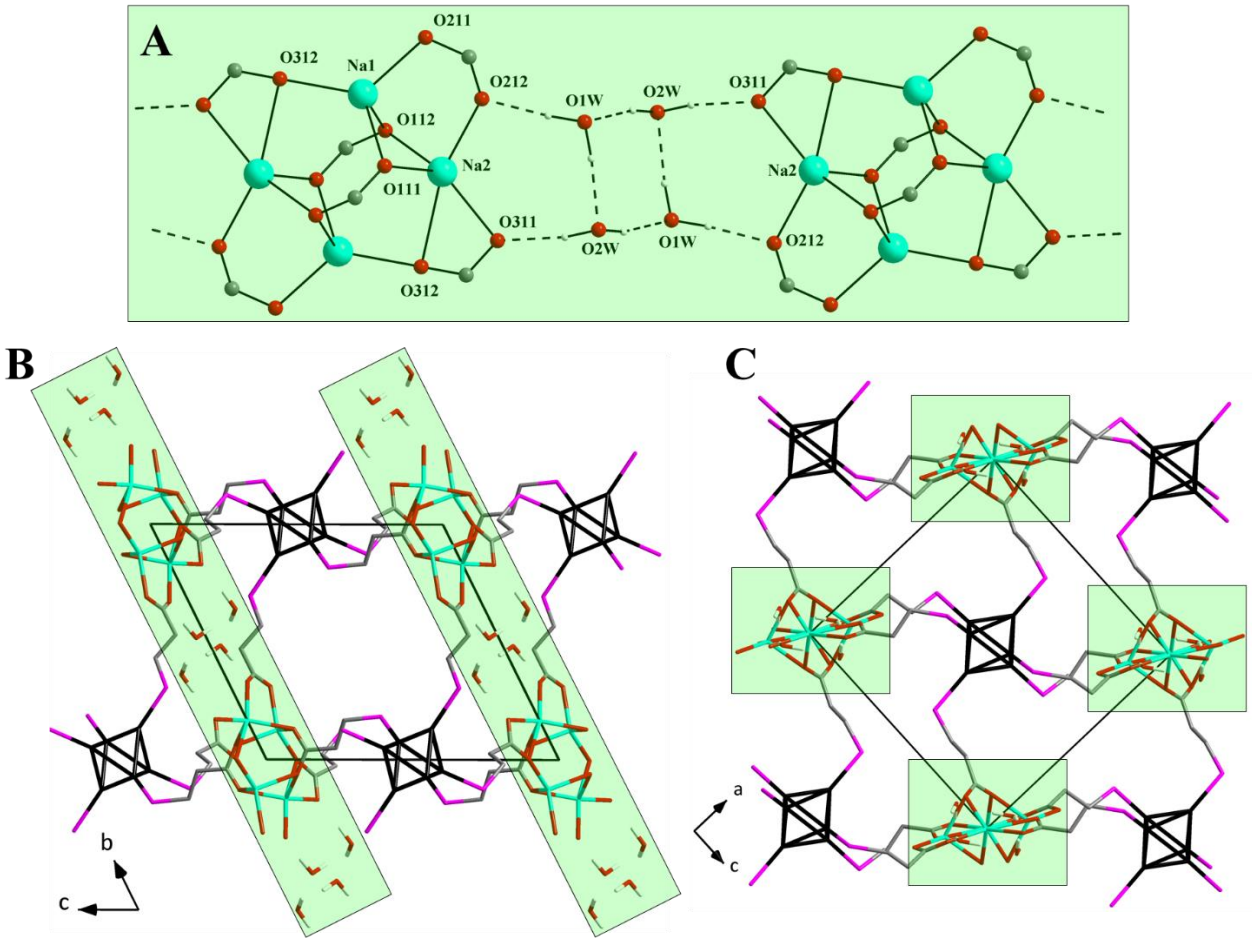

Figure 11S. Non-porous 3D-coordination polymer based on octahedral clusters and alkali metals observed in the Na_4-**1**·$4H_2O$ and Na_4-**2**·$4H_2O$ structures.

Table 3S. The Na–O and hydrogen bond lengths in Na_4-**1**·$4H_2O$ and Na_4-**2**·$4H_2O$.

Contact	Na_4-**1**·$4H_2O$ (Å)	Na_4-**2**·$4H_2O$ (Å)
O1W···O212	2.774	2.771
O2W···O311	2.804	2.825
O1W···O2W	2.764 and 2.890	2.780 and 2.895
Na1···O111	2.297	2.289
Na1···O112	2.357	2.367
Na1···O211	2.262	2.257
Na1···O312	2.231	2.227
Na2···O111	2.347	2.368
Na2···O112	2.364	2.384
Na2···O212	2.265	2.293
Na2···O311	2.313	2.308
Na2···O312	2.615	2.696

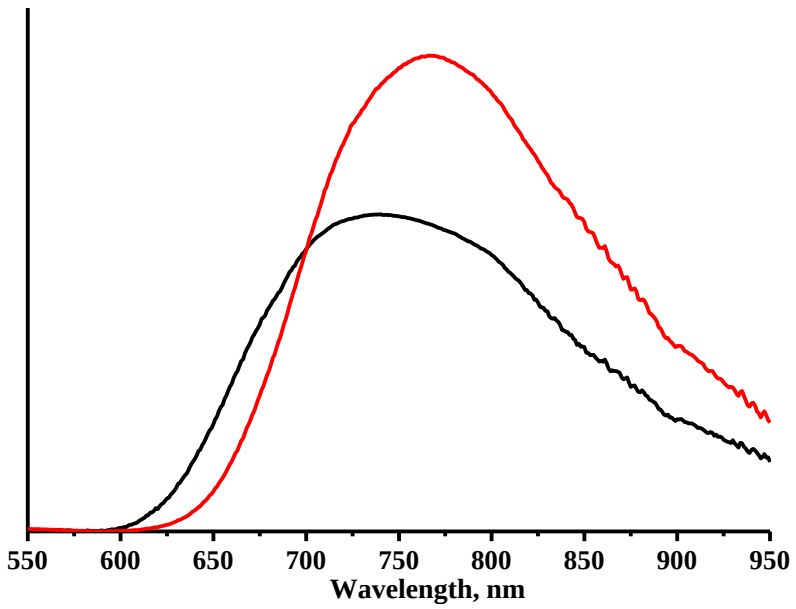

Figure 12S. Emission spectra of acetonitrile solutions of H_4-**1**·2HBr·H_2O (black line) and H_4-**2**·2HBr·H_2O (red line) under oxygen-free conditions.

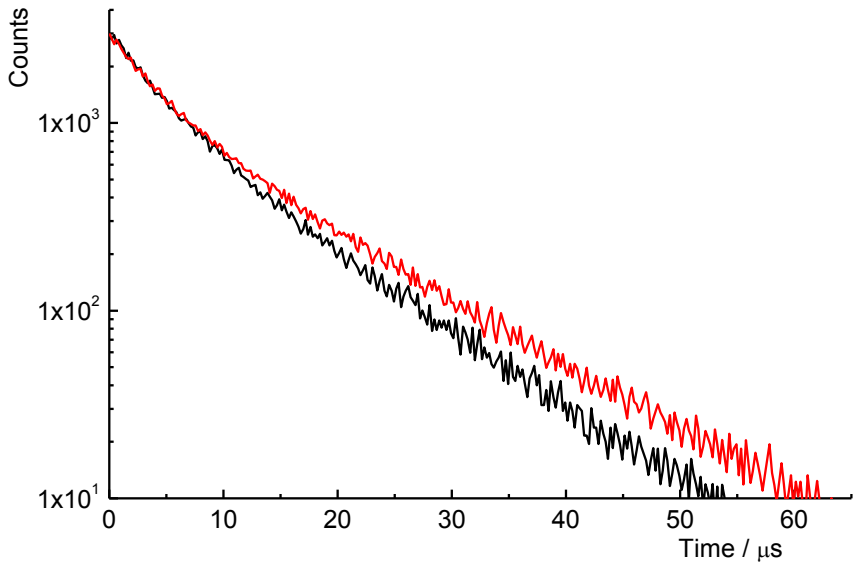

Figure 13S. Luminescence decay curves of powdered H_4-**1**·2HBr·H_2O (black line) and H_4-**2**·2HBr·H_2O (red line).

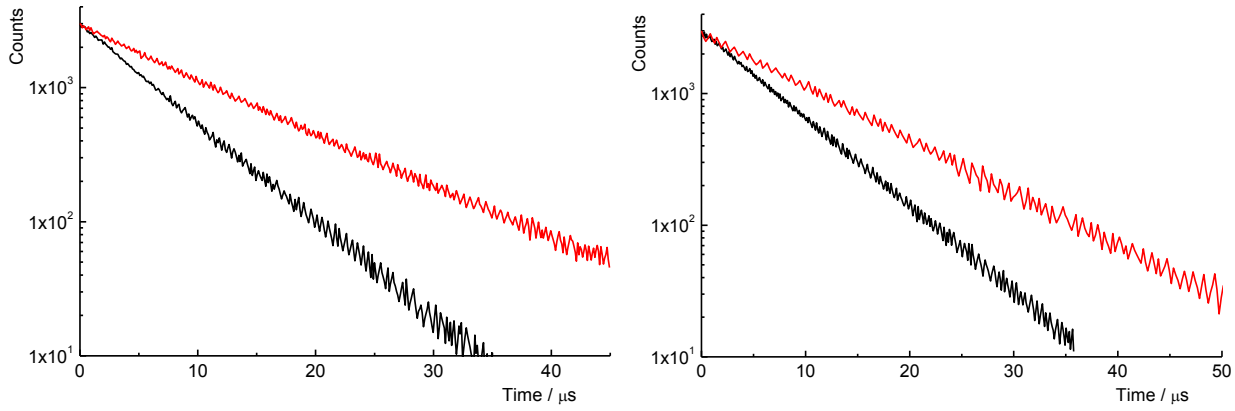

Figure 14S. Luminescence decay curves of aerated (left) and deaerated (right) acetonitrile solutions of H_4-**1**·2HBr·H_2O (black line) and H_4-**2**·2HBr·H_2O (red line).

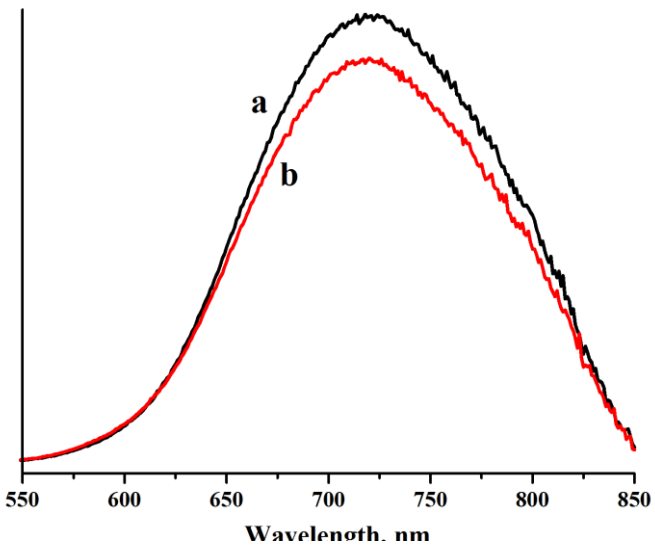

Figure 15S. Luminescence spectra of H_4-**1**·2HBr·H_2O in argon- (a) and oxygen-saturated (b) PBS.

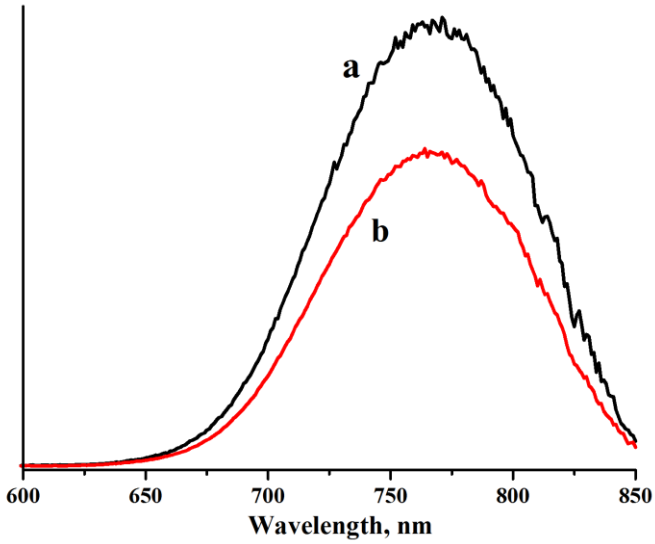

Figure 16S. Luminescence spectra of H_4-**2**·2HBr·H_2O in argon- (a) and oxygen-saturated (b) PBS.

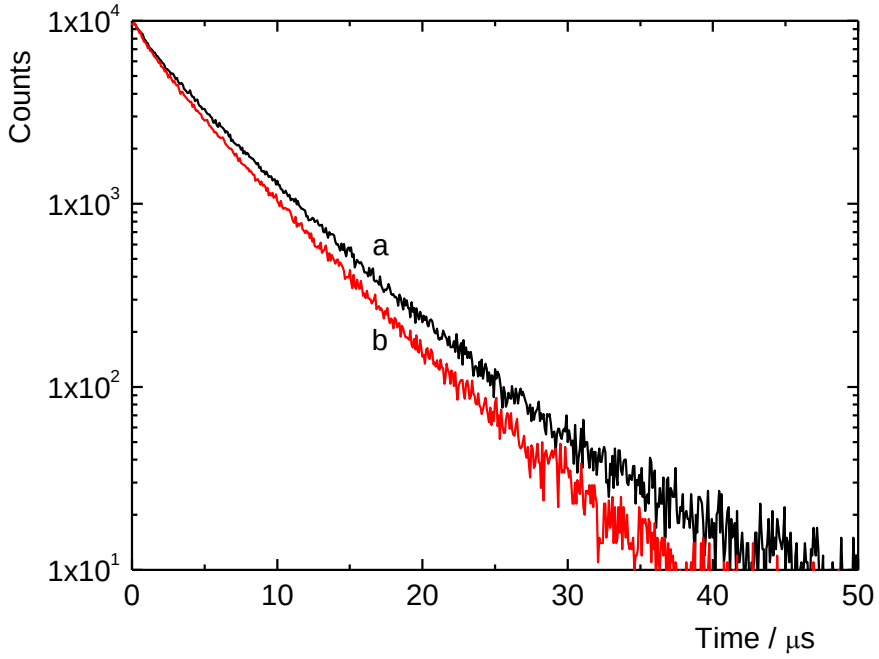

Figure 17S. Luminescence decay curves of H_4-**1**·2HBr·H_2O recorded at 720 nm in argon- (a) and oxygen-saturated (b) PBS.

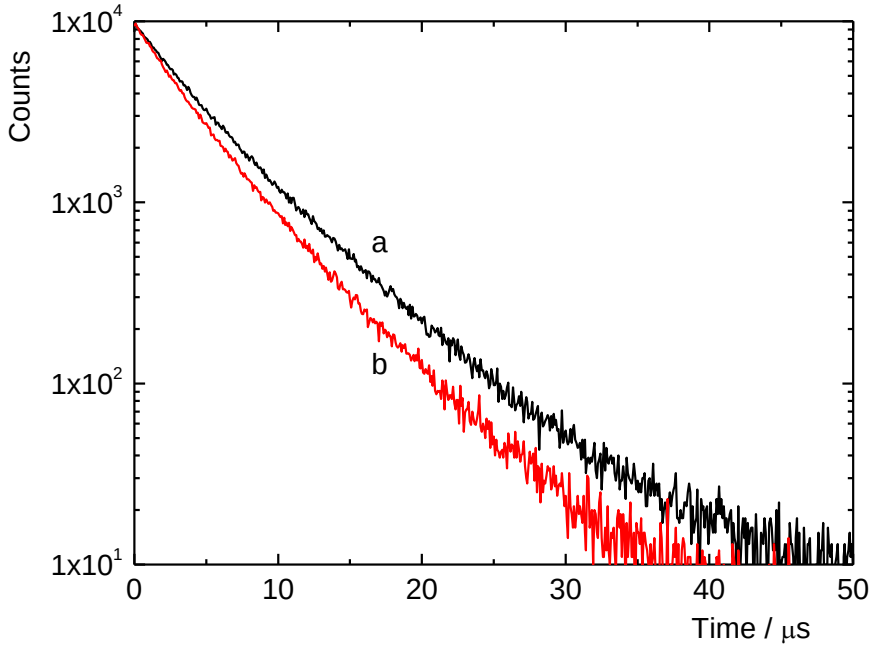

Figure 18S. Luminescence decay curves of H_4-**2**·2HBr·H_2O recorded at 765 nm in argon- (a) and oxygen-saturated (b) PBS.

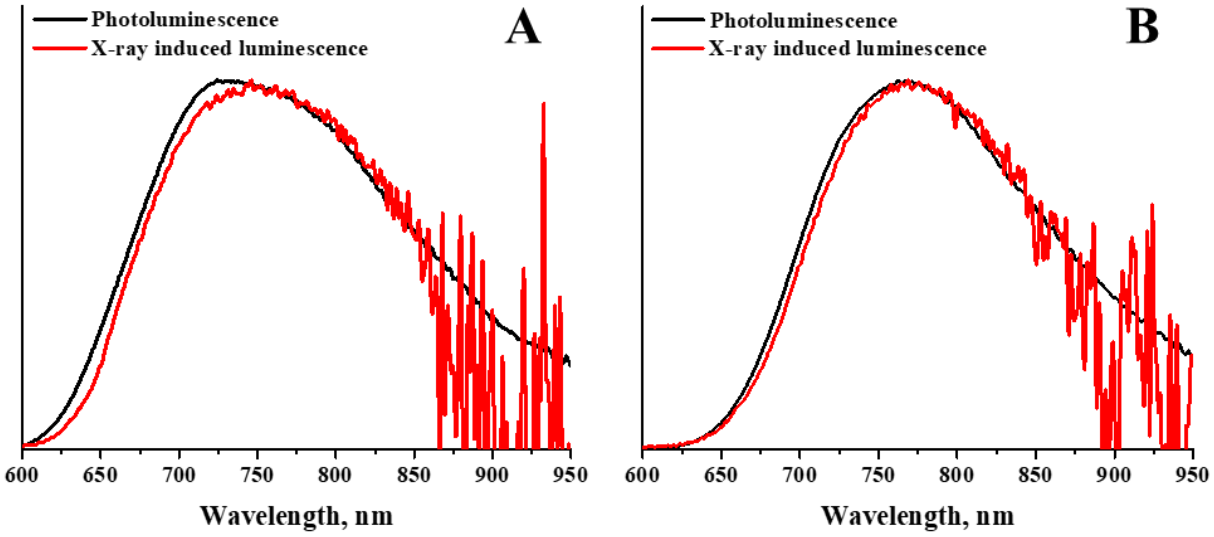

Figure 19S. Photoluminescence and X-ray excited optical luminescence (XEOL) spectra of H_4-**1**·2HBr·H_2O (A) and H_4-**2**·2HBr·H_2O (B) powders.

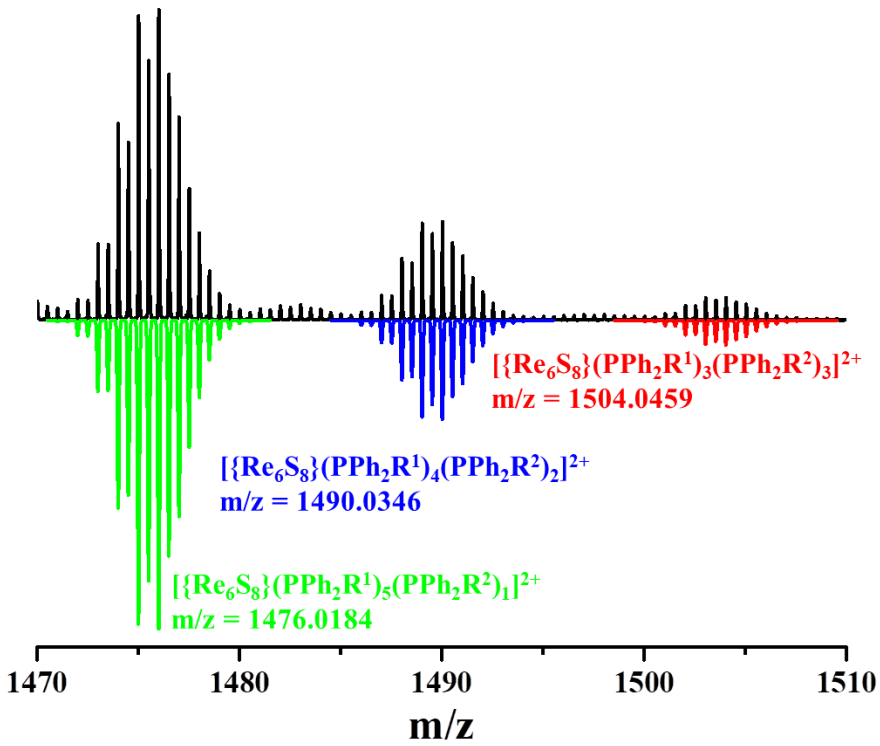

Figure 20S. Fragment of HR-ESI-MS of H_4-**1**·2HBr in ethanol containing HBr (black) and corresponding simulation (coloured). R^1 = CH_2CH_2COOH, R^2 = CH_2CH_2COOEt. Measured m/z values correspond to theoretical values: 1476.0116, 1490.0273 and 1504.0429 from left to right.

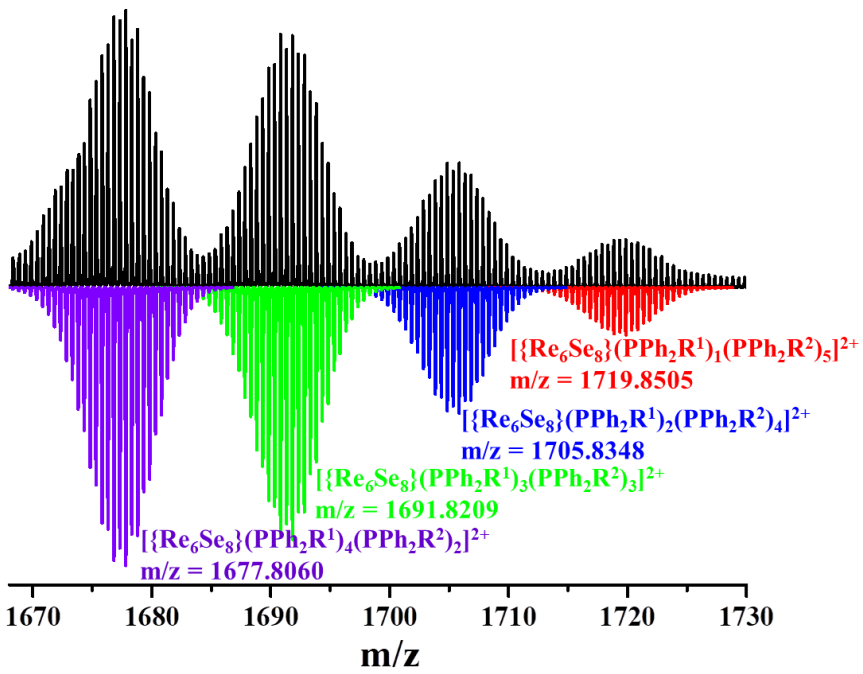

Figure 21S. Fragment of HR-ESI-MS of H_4-**2**·2HBr in ethanol containing HBr (black) and corresponding simulation (coloured). R^1 = CH_2CH_2COOH, R^2 = CH_2CH_2COOEt. Measured m/z values correspond to theoretical values: 1677.8082, 1691.8239, 1705.8396 from left to right.

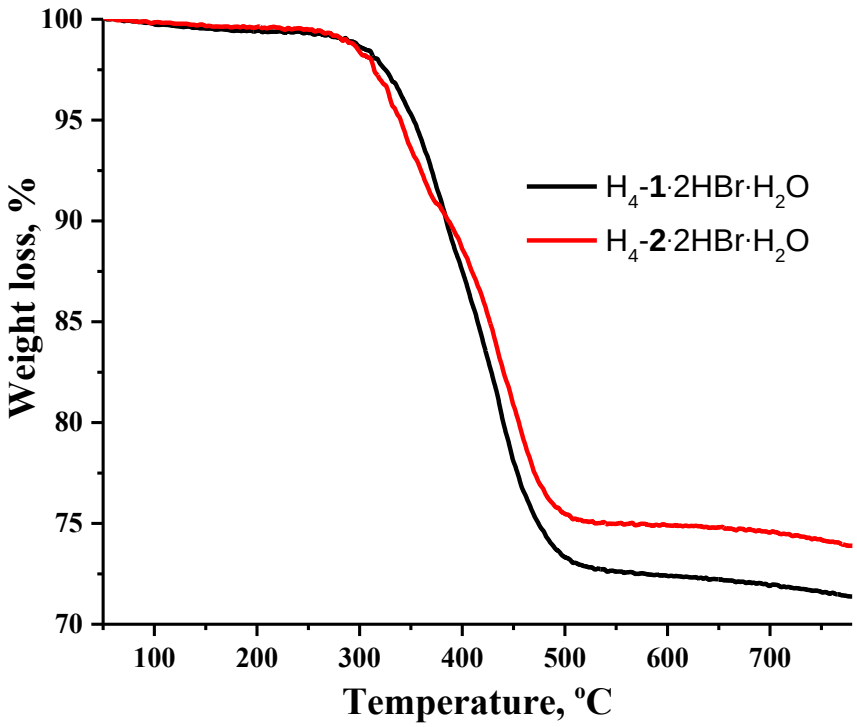

Figure 22S. TGA curves of H_4-**1**·2HBr·H_2O and H_4-**2**·2HBr·H_2O. Heating rates are 10° C·min^{-1}.

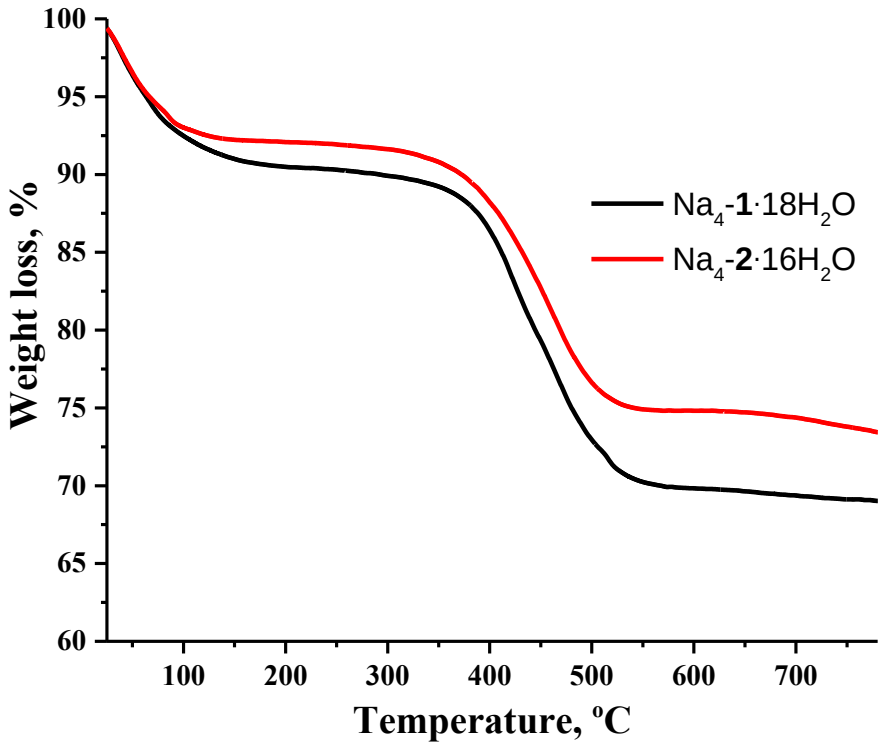

Figure 23S. TGA curves of Na_4-**1**·$18H_2O$ and Na_4-**2**·$16H_2O$. Heating rates are 10° C·min^{-1}.

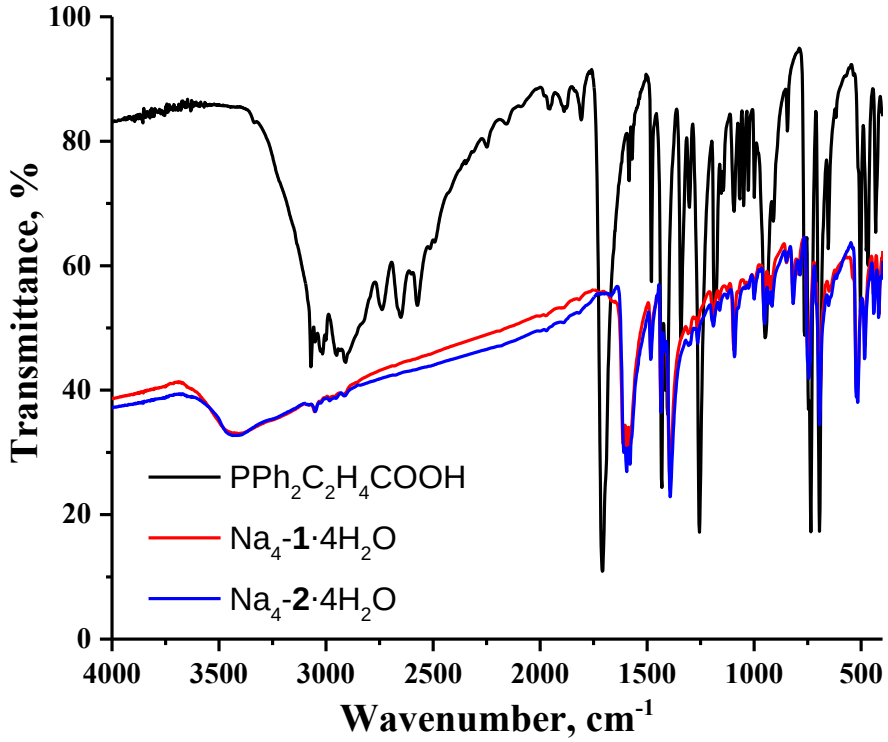

Figure 24S. FTIR spectra of Na_4-**1**·$4H_2O$ and Na_4-**2**·$4H_2O$ compared with that of the ligands, i.e., (2-carboxyethyl)diphenylphosphine.

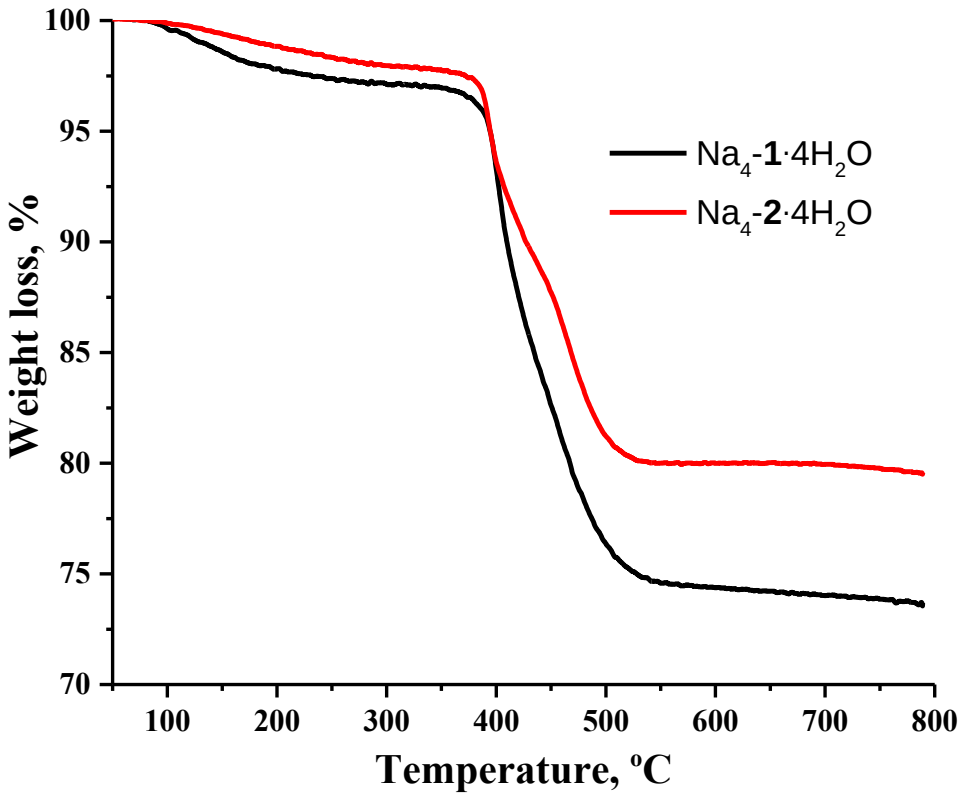

Figure 25S. TGA curves of Na_4-**1**·$4H_2O$ and Na_4-**2**·$4H_2O$. Heating rates of 10° C·min^{-1}.